Dipion Production at Low Momentum Transfer in π^--p Collisions at 1.5 BeV/c*

A. R. Clark,† J. H. Christenson,‡ J. W. Cronin, and R. Turlay§

Palmer Physical Laboratory, Princeton University, Princeton, New Jersey

(Received 3 May 1965)

We have used precision spark-chamber spectrometers to measure the dipion mass spectrum from the reaction $\pi^-+p \to \pi^-+\pi^++n$ at an incident momentum of 1.5 BeV/c. The spectrum was observed between 450 and 1000 MeV, with π-π scattering angles at 90±5 deg, and with four-momentum transfer to the nucleon between the minimum Δ_{min} and $\Delta_{min}+2\mu$. The mass resolution of the apparatus was ±4 MeV. With more than 6000 events we observe a peak in the π-π mass spectrum at ~750 MeV with a width $\Gamma \cong 130$ MeV. We do not observe any other structure in the mass range explored. With these results we can set an upper limit for the branching ratio ($\omega \to \pi^+\pi^-/\omega \to \pi^+\pi^-\pi^0$) of $\leq 1.0\%$, based on the assumption that there is no interference between the ρ and ω amplitudes. Interpreting the data with the one-pion exchange (OPE) model, we have computed the differential cross section $d\sigma_{\pi\pi}/d \cos\theta_{\pi\pi}$ at 90 deg. This quantity shows a strong peak at the mass of the ρ^0 meson, but the peak is much larger than expected from a $J=1$ π-π resonant state produced by OPE. If this peak is really the ρ^0 meson, we must be observing it because of absorption phenomena in the initial π-N and final ρ-N states which tend to depolarize the ρ. Expressing the ρ decay intensity as $a+b \cos^2\theta_{\pi\pi}$, our data require $a/b \approx 0.06$, while the simple OPE model predicts $a/b=0$. Other features of the data, the momentum-transfer distribution and the Treiman-Yang angular distribution, fit the OPE predictions fairly well. We discuss some evidence that the effect of a 1.4-BeV, $T=\frac{3}{2}$ isobar can be seen in the data.

I. INTRODUCTION

THE original motivation for this experiment was stimulated by reports of possible structure in the ρ-meson peak and by reports of other possible π-π resonances. While most experiments have shown the ρ to be a single peak in the π-π mass spectrum centered around 750 MeV with a width Γ of the order of 110 MeV,[1] a Berkeley group[2] found indications of two peaks at 720 and 780 MeV in the spectrum from $p+\bar{p} \to 2\pi^+ +2\pi^-+m\pi^0$. Similar structure in the ρ region has been observed since then in the data from π^--p interactions[3-6] and K^--p interactions.[7] Efforts have been made to interpret this structure as ρ-ω interference or as evidence for a 2π decay of the ω meson.[8,9] At the present time a survey[10] of a large amount of data indicates that the rate $(\omega \to \pi^++\pi^-)/(\omega \to \pi^++\pi^-+\pi^0)$ is

probably less than 1%. A second $\pi^+-\pi^-$ resonance with a mass of 560 MeV was reported by Barloutaud et al.[11] and supporting evidence was given by Zorn.[12] However, this state has not been observed in several other experiments.[1]

In order to exploit the spark chamber technique in this study, we sought an arrangement which was selective for the reaction $\pi^-+p \to \pi^++\pi^-+n$ at low momentum transfer. The reaction was observed for those events in which the two pions were emitted symmetrically in the laboratory system with respect to the incident beam. This limited geometry allowed one to observe the desired low-momentum-transfer events with a very small contamination of multiple-pion-production events. The arrangement has the serious restriction that the angular range in $\cos\theta_{\pi\pi}$ was limited to ± 0.4 about zero, where $\theta_{\pi\pi}$ is the π-π scattering angle. Such a restriction biases strongly against the ρ meson if it is produced by a perfect one-pion exchange (OPE) process, since the decay angular distribution for that process is $W(\theta)=\cos^2\theta_{\pi\pi}$. Thus our method has a good efficiency for observing $J=0$ resonances which are isotropic in $\cos\theta_{\pi\pi}$, but a rather small efficiency for $J=1$ resonances which are generated only by an OPE process.

The observation of the π-π mass spectrum in the region of $\cos\theta_{\pi\pi}=0$ gives conditions that are particularly favorable for observing the 2π decay of the ω^0. The simplest production mechanisms for the ρ^0 (OPE) and the ω^0 (ρ exchange) give decay angular distributions of $\cos^2\theta_{\pi\pi}$ and $\sin^2\theta_{\pi\pi}$, respectively, for a vector particle decaying to two pions.[13] Furthermore, for this simplified mechanism there is no interference between the two amplitudes. Thus the effect of the 2π decay of the ω

† Present address: Lawrence Radiation Laboratory, Berkeley, California.
‡ Present address: Columbia University, New York, New York.
§ Present address: Centre d'Études Nucléaires de Saclay, France.

[1] M. Roos, Rev. Mod. Phys. 35, 314 (1963).
[2] J. Button, G. R. Kalbfleisch, G. R. Lynch, B. C. Maglić, A. H. Rosenfeld, and M. L. Stevenson, Phys. Rev. 126, 1858 (1962).
[3] W. Walker, E. West, A. Erwin, and R. March, *Proceedings of the 1962 International Conference on High-Energy Physics, Geneva* (CERN Scientific Information Service, Geneva, Switzerland, 1962), p. 371.
[4] W. Fickinger, D. Robinson, and E. Salant, Phys. Rev. Letters 10, 457 (1963).
[5] Saclay-Orsay-Bari-Bologna Collaboration, Nuovo Cimento 29, 515 (1963).
[6] D. Keefe, L. T. Kerth, C. M. Noble, J. J. Thresher, W. A. Wenzel, and T. F. Zipf, University of California Radiation Laboratory Report No. UCRL-11468, 1964 (unpublished).
[7] D. Huwe, University of California Radiation Laboratory Report No. UCRL-11291, 1964 (unpublished).
[8] S. L. Glashow, Phys. Rev. Letters 7, 469 (1961).
[9] J. Bernstein and G. Feinberg, Nuovo Cimento 25, 1343 (1962).
[10] G. Lütjens and J. Steinberger, Phys. Rev. Letters 12, 517 (1964).
[11] R. Barloutaud, J. Heughebaert, A. Levéque, C. Loudec, J. Meyer, and D. Tycho, Nuovo Cimento 27, 238 (1963).
[12] B. Sechi Zorn, Phys. Rev. Letters 8, 282 (1962).
[13] M. M. Islam and R. Piñon, Phys. Rev. Letters 12, 310 (1964).

should be enhanced relative to the ρ. The above arguments depend of course on a specific model and suggest only that the particular experimental conditions we have chosen may have a good chance to display the effect.

The incident pion momentum of 1.5 BeV/c was a compromise between the availability of high-intensity high-momentum beams at the Cosmotron and the desire to be able to compare this study in a limited range with the more extensive work of the Saclay-Orsay-Bari-Bologna Collaboration[5] at 1.6 BeV/c and the work of Fickinger et al.[4] at 1.7 BeV/c.

II. EXPERIMENTAL APPARATUS

A system of six spark chambers and three magnets was arranged to analyze the momenta of the incident pion and the two secondary pions in the reaction $\pi^- + p \rightarrow \pi^- + \pi^+ + n$. A knowledge of these three vector momenta is sufficient to allow complete kinematical reconstruction of the event, and permits multiple-pion production events to be discarded on the basis of the calculated missing mass.

A diagram of the apparatus is shown in Fig. 1. Thin plate spark chambers were placed at each end of the last bending magnet in the beam transport system to measure the vector momentum of the incident pion. The interaction took place in a 4-ft-long×6-in.-diameter liquid-hydrogen target, and the vector momenta of the two secondary pions were measured in spark chamber spectrometer systems placed symmetrically on either side of the beam axis. Each spectrometer system (magnet, spark chambers, and optics) was mounted on a cart so that it could be moved relatively easily during the experiment to cover a wide range of dipion opening angles.

Scintillation counters (S_1,S_2) were placed downstream of each spectrometer to indicate the passage of a particle through the system. Water Cerenkov counters (C_1,C_2) were located immediately behind each scintillator to reject recoil protons from elastically scattered pions. A scintillation counter with a 6-in. hole in the center (S_3) was placed in front of the target and run in anti-coincidence with the other counters to eliminate interactions occurring in the walls of the target vacuum box. The spark chambers were fired and photographed whenever a fourfold coincidence signal $S_1S_2C_1C_2$ was received, with no count in S_3. Tests made on the composite counter system showed it to be more than 99% efficient for detecting pions in our energy range.

Each of the decay pion spectrometers consisted of a bending magnet with thin-plate spark chambers mounted at each end to determine the trajectory of the particles as they entered and left the field region. The magnets used were standard 18-in.×36-in. AGS picture-frame magnets with a 6-in. gap. These magnets were chosen primarily for their extremely uniform field, which was measured to 0.1%. The two magnets were powered
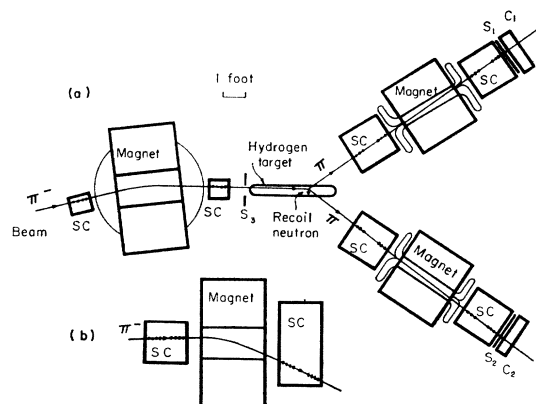

FIG. 1. Schematic views of the experimental apparatus. (a) Plan view, showing all spark chambers and analyzing magnets; (b) side view of one decay pion spectrometer. "SC" denotes spark chamber.

in series to ensure that the two fields would track together; the current was regulated by a temperature-compensated Hall probe mounted in one magnet. A nuclear magnetic resonance probe was mounted in the other magnet as an independent monitor of the field.

The spark chambers were designed to place a minimum amount of material in the path of a particle traversing them. The plates were made by gluing a 0.001-in. Al foil to each side of 0.5-in.-thick Al frames. Each chamber had ten plates mounted in two banks of five plates each, with $\frac{3}{8}$-in. gaps between the plates. The banks were separated by 16 in., giving a good lever arm for angular measurements. Each plate assembly, surrounded by a self-calibrating set of fiducial reticules, was mounted in a gas-tight chamber filled with a gas mixture of 90% Ne-10% He. Particles entered and left the chambers through 0.005-in. Mylar windows.

In order to make each spectrometer a self-contained unit, the spark chambers were accurately positioned on platforms attached directly to the magnets; a camera and the optical system necessary to photograph orthogonal views of each chamber were also mounted on each magnet. Since the magnets were mounted on carts, this arrangement made it possible to move the spectrometers several times during the experiment without having to realign the spark chambers and optical systems.

A more detailed description of the spectrometers and other apparatus is given in Ref. 14.

III. EXPERIMENTAL PROCEDURE

The experiment was performed at the Brookhaven National Laboratory Cosmotron during the winter and spring of 1963. The cosmotron was run at an internal energy of 3 BeV with an average circulating beam of $\sim 10^{11}$ protons per pulse. A drawing of the pion beam and the experimental layout is shown in Fig. 2. The

[14] A. R. Clark, Princeton University, Elementary Particles Laboratory Technical Report No. 35, 1964 (unpublished).
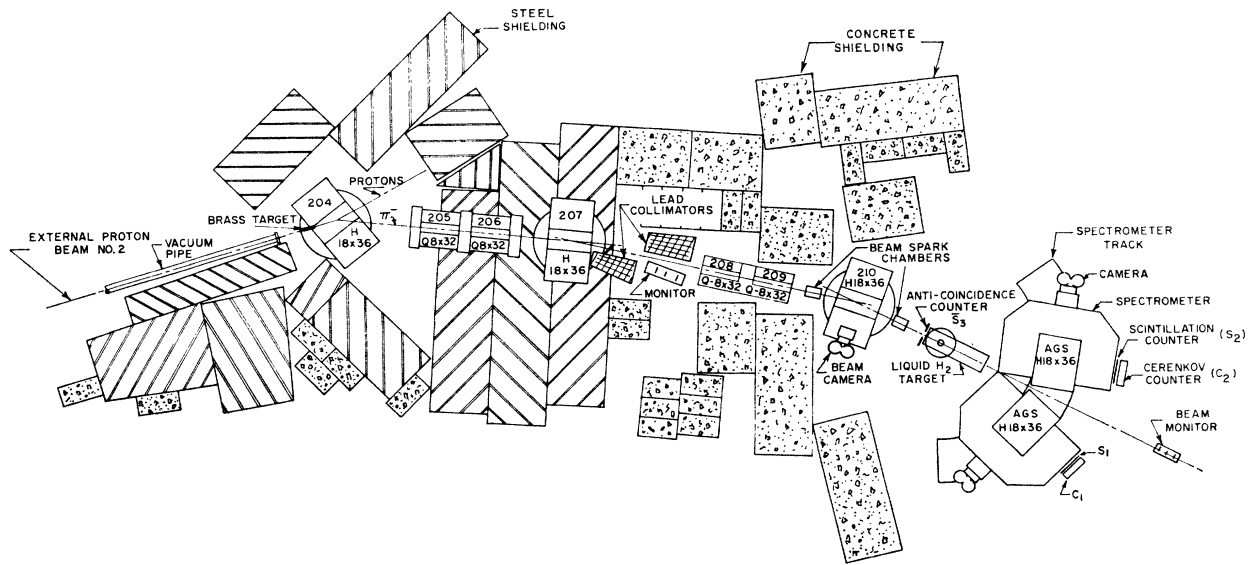
FIG. 2. Layout of pion beam and experimental apparatus at the Cosmotron.

external proton beam was focused onto a brass target; forward-produced pions were focused and momentum analyzed by a system of magnets, resulting in a beam of momentum 1.52 ± 0.15 BeV/c at an intensity of 1.5×10^5 pions per 10^{11} protons in the circulating beam. Muon contamination was estimated at $(10\pm4)\%$. The focusing magnets were set to give a vertical focus at the hydrogen target center and a horizontal focus at infinity.

The beam was monitored by a three-counter telescope located on the beam axis beyond the experimental setup. This was calibrated at the beginning of each data run by temporarily installing additional counters in front of the hydrogen target to directly measure the pion flux. A second telescope downstream of the second bending magnet (see Fig. 2) was used to check the measurements and to correct the primary monitor for the removal of the calibration counters. In addition, a small single counter mounted adjacent to the primary monitor was used as a short-term reference to evaluate saturation effects in the other monitors. During the calibration procedure for each data run, 500 to 700 pictures of the beam spark chambers were taken to study the structure of the beam in greater detail.

Because of the small solid angle subtended by the spectrometer magnets, the range in dipion mass (m^*) which could be observed at a given setting of the spectrometers was restricted to a 300-MeV interval. To observe the full dipion mass spectrum, data were taken with the spectrometers at three different angles with respect to the beam line. The angles and mass ranges covered were:

Geometry	Mass range
17 deg	$430<m^*<700$ MeV
27 deg	$600<m^*<900$ MeV
33 deg	$700<m^*<1000$ MeV

The total incident pion flux was divided among the three geometries such that we would have obtained roughly the same number of events at each setting if the data were dominated by phase space. The event rate varied from 0.1 to 0.6 events per pulse, depending on the geometry.

The integrated pion flux incident at each geometry was calculated from the beam monitors and corrected for the muon contamination. Additional corrections were necessary, however, to obtain the effective pion flux which produced the events actually observed. Anti-coincidence accidentals from the beam defining counter S_3 effectively gated the electronics off during part of the beam spill (8% loss). Corrections were made for event losses due to scanning inefficiency (1%) and for absorption and μ decay of the secondary pions within the spectrometers (11% and 13%, respectively). The particular losses indicated in parentheses are given for the 27° geometry; the corrections are slightly different for the other geometries. Finally, the spark chambers were known to be inefficient during part of the experimental run. Since the inefficiencies only reduced the number of measurable events without introducing any bias to the data, the integrated flux was calculated at each geometry for that part of the data where the spark chambers were known to be fully efficient and then scaled to account for the total number of events observed. The corrected integrated flux at each geometry was:

Geometry	Effective integrated flux
17 deg	$(6.73\pm0.60)\times10^9$ pions
27 deg	$(1.20\pm0.11)\times10^{10}$ pions
33 deg	$(1.19\pm0.10)\times10^{10}$ pions

The error in each case is the absolute error; the ratio between any two geometries is known to about $\pm3\%$.

The data for each event were recorded on three frames of film—a picture of the beam spectrometer and a picture of each decay pion spectrometer. A typical picture of a good track in one of the decay spectrometers is shown in Fig. 3. The two banks of the upstream chamber appear on the right, and those of the larger downstream chamber on the left. The top view of each bank is seen above the side view. A negative pion is seen entering horizontally from the right; after being deflected downward by the magnet, it passes through the large chamber at a fairly steep angle. There is no deflection in the top view. The sparks are seen superimposed on the grids of the front and top fiducial reticules, which were the only ones illuminated under normal conditions. Complete pictures of all the reticules around each chamber were taken at the beginning and end of each roll of film for calibration of the optical system.

A total of 40 000 exposures were taken during the run. About 30% of these showed a track in each secondary spectrometer and were measured as possible dipion events. The remaining pictures could easily be rejected during scanning by the absence of a track in one or more of the spark chambers. Out of the 12 000 possible events, ∼50% were successfully analyzed as good events. The other 50% were rejected primarily because one of the tracks either scattered within the system or passed through a corner of a magnet yoke. The remaining 70% of the data were consistent with the expected background from accidental triggers due to stray radiation.

Unfortunately, the incident pion flux required to maintain a reasonable event rate caused the beam spark chambers to saturate rather badly. As a result, the momentum of the incident pion, which is necessary for complete event reconstruction, was measured for only 17% of the data. However, this sample was sufficient to show that we could safely assume the missing mass to be a neutron for analysis of the other data. This problem will be discussed in more detail below.

IV. DATA REDUCTION

The film was scanned and measured on a Hydel x-y measuring machine, which gave a projected image roughly $\frac{1}{4}$ life size. The scanning criteria were kept to a minimum to avoid biases; the general philosophy was to let the computer, rather than the scanner, decide if an event was good or not. Each event that showed a complete track in each decay pion spectrometer was measured; the corresponding beam spectrometer picture was measured if it contained a good track.

For each event the x and y coordinates of several fiducial intersections and each visible spark were measured and punched onto IBM cards. The data cards were processed on an IBM 7094 computer by a series of programs which reconstructed the spatial coordinates of the sparks, momentum analyzed the track in each

Fig. 3. Typical data picture, showing a negative pion passing through one spectrometer.

spectrometer, and reconstructed each event kinematically. A detailed description of these various steps is given in Ref. 14.

The uncertainties in the momentum analysis and the dipion mass calculation were caused primarily by multiple scattering; measurement errors were negligible. (Discussions of the measurement and spatial reconstruction accuracy can be found in Ref. 14 and 15.) Multiple scattering calculations led to an expected dipion mass resolution of ±3.5—4.0 MeV, depending on the dipion mass and the spectrometer geometry. About half of the uncertainty was due to scattering of the pions in the hydrogen as they left the target; the remaining effect was caused by a momentum uncertainty from scattering within the spectrometer systems.

The resolution and absolute mass calibration were checked in two ways. Seven K°_1's associated with the missing mass of a Λ° were identified in the data; the statistics are rather meager, but we find a K° mass of 498.4 MeV with a standard deviation of 4.9 MeV. Data from another experiment, which used the same spectrometers in a similar configuration to study K°_1 regeneration,[16] were also measured and analyzed with our programs to check resolution. Multiple scattering predicted a mass resolution of ±3.7 MeV for $K^\circ_1 \to \pi^+\pi^-$. A sample of 181 events gave a K°_1 mass of 498.4 MeV with a standard deviation of 4.6 MeV for an individual measurement.

[15] J. H. Christenson, A. R. Clark, and J. W. Cronin, IEEE Trans. Nucl. Sci. 11, 310 (1964).
[16] J. H. Christenson, Princeton University, Elementary Particles Laboratory Technical Report No. 34, 1964 (unpublished).
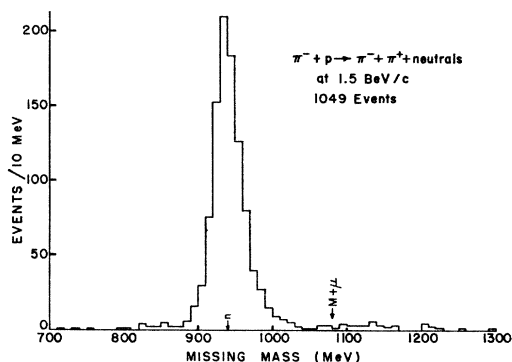
FIG. 4. Missing mass spectrum for all type-I events.

For kinematic reconstruction, each event was classified as type I if the incident-pion momentum had been measured and as type II if only the two decay pions were seen. The type-I events were overdetermined kinematically and permitted calculation of the missing mass, assuming a more general reaction of the form $\pi^- + p \rightarrow \pi^- + \pi^+ + X^\circ$. The missing mass distribution for all type-I events is shown in Fig. 4. The spectrum shows a dominant neutron peak; the full width at half-maximum of 40 MeV indicates an uncertainty of $\sim 2\%$ in the measurement of the incident pion momentum. The spectrum also shows a contamination of 4.1% from multiple pion production events, which are identified as having a missing mass (M_m) greater than $M + \mu$, where M and μ are the nucleon and pion masses, respectively. Attempts to remove this background will be discussed below. The type-I events were also reconstructed with a constrained neutron mass for further analysis.

The measurements for the type-II events were sufficient to calculate the dipion mass and vector momen-
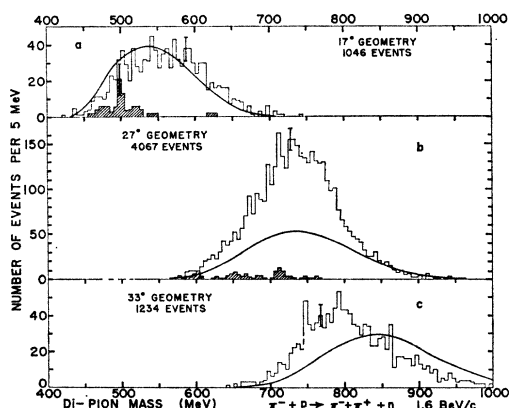

FIG. 5. Dipion mass spectra obtained at each geometry. (a) Spectrometers set at 17 deg to beam axis; (b) 27 deg; (c) 33 deg. The shaded areas show the estimated contamination from multiple pion production events. The smooth curves show the spectra we would see at each geometry if the production cross section were independent of m^*, Δ^2, and $\cos\theta_{\pi\pi}$; the shape of these curves is determined primarily by the geometrical biases.

tum, but it was necessary to assume that the missing particle was a neutron and that the incident pion was traveling parallel to the target axis to complete the kinematic reconstruction. The first assumption was justified by the low contamination observed in the type-I events. Studies of the beam show that assuming the beam direction to be parallel to the target axis introduced an error of less than 1 deg for 80% of the events and introduced a mean error of $\pm 3\%$ to the calculated four momentum transfer Δ. Because of the constrained neutron mass, this error in Δ is about the same as that obtained for unconstrained type-I events.

The dipion mass (m^*) distributions obtained at each geometry are shown in Fig. 5, including both type-I and -II events. The shaded areas show the estimated contributions to the spectra from the multiple-pion-production events. These distributions were obtained by examining the m^* mass spectrum for the fraction of type-I events with $M_m > M + \mu$ for each geometry, and scaling the curves up to the same fraction of the total number of events. Accordingly, the statistics are rather poor; the contamination curves are based on 18 and 25 events at the 17° and 27° geometries, respectively. No contamination was observed at 33°. The distribution of the contamination events at each geometry is consistent with the kinematics of a three-pion final state. The peak at 500 MeV in the 17° data is caused by the presence of a few K°'s from $K^\circ - \Lambda$ associated production.

In order to determine the geometrical biases imposed on the data by the apparatus, a Monte-Carlo program was written to calculate the detection efficiency for each geometry as a function of m^*, Δ, and $\cos\theta_{\pi\pi}$, where m^* is the invariant dipion mass, Δ is the four-momentum transfer to the nucleon, and $\theta_{\pi\pi}$ is the π-π scattering angle. $\theta_{\pi\pi}$ is defined as the angle between the incident and final π^- momentum vectors in the dipion rest frame.

The program constructed a large number of events for selected values of m^*, Δ, and $\cos\theta_{\pi\pi}$, choosing the other necessary parameters at random from appropriate distributions. The momentum, direction, and target entry coordinates for the incident pion were picked from a random sample of real beam particles obtained from the beam pictures taken during the monitor calibrations; this procedure conserved any correlations which existed between these variables. The interaction point was chosen uniformly along the path through the target, and a correction applied for attenuation of the beam in the target. The azimuthal angles of the dipion production plane and the π-π scattering plane were chosen uniformly between 0 and 2π. The event was then constructed in space relative to the apparatus, and the trajectory of each decay pion was traced to determine if the event would have been detected. The efficiency for these values of m^*, Δ, and $\cos\theta_{\pi\pi}$ is then defined as the number of events accepted divided by the total number tried. Enough events were tried at each point so that the statistical uncertainty in the efficiency was always

FIG. 6. Total dipion mass spectrum obtained by adding the data obtained at each geometry after subtraction of the estimated multiple pion production events. The events are restricted by the geometrical biases to $\Delta < \Delta_{min} + 2\mu$ and $|\cos\theta_{\pi\pi}| < {\sim}0.4$. The smooth curve is invariant phase space, arbitrarily normalized. The inset shows the data for $750 < m^* < 820$ MeV on an enlarged scale, with a smooth curve fit to the points.
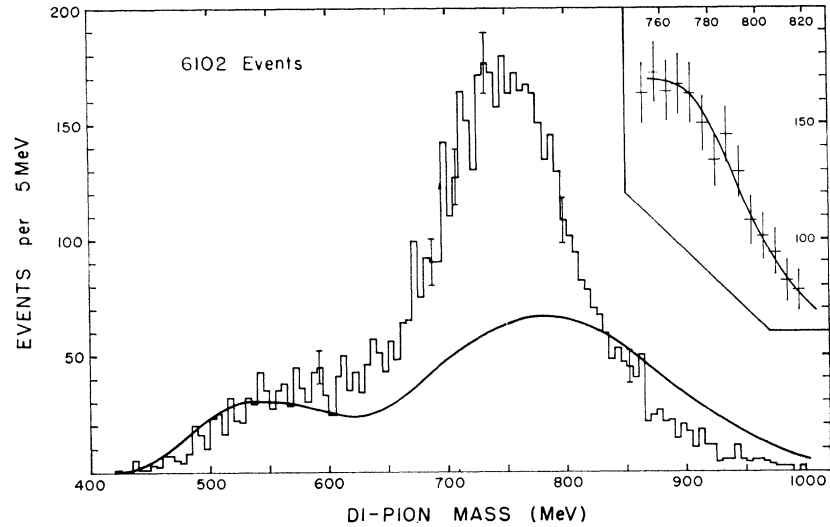
less than 10% of the uncertainty in the experimental data at that point. The efficiency calculated in this manner represents a weighted average over the incident momentum distribution; this averaging will have some effect on the calculation of the π-π cross section, which is discussed in more detail below.

The calculations showed that we could see dipions with masses within roughly a 300-MeV-wide band for a particular setting of the spectrometers; the cutoffs are due to the variation of the dipion lab opening angle with m^*. This effect is shown in Fig. 5; the smooth curves show the mass distributions which we would observe if the production cross section were independent of m^*, Δ^2, and $\cos\theta_{\pi\pi}$. The three curves are weighted relative to each other by the total pion flux at their respective geometries, but the over-all normalization is arbitrary.

For any value of m^*, the efficiency is at a maximum for $\Delta = \Delta_{min}$ (forward produced dipions) and falls to zero in the vicinity of $\Delta = \Delta_{min} + 2\mu$. As a function of $\theta_{\pi\pi}$, the efficiency has its maximum value for $\cos\theta_{\pi\pi} = 0$, it falls to 50% of its peak value for $\cos\theta_{\pi\pi} \sim \pm 0.2$, and it goes to zero for $\cos\theta_{\pi\pi} \sim \pm 0.5$. These limits on $\cos\theta_{\pi\pi}$ are somewhat unfortunate because they tend to enhance the $J=0$ contribution of the π-π cross section relative to the higher angular-momentum states. In particular, $J=1$ states which decay with a $\cos^2\theta_{\pi\pi}$ dependence, such as the ρ meson, are strongly suppressed.

V. RESULTS AND DISCUSSION

The total dipion mass spectrum is shown in Fig. 6. The histogram is a sum of the three experimental distributions shown in Fig. 5, with the estimated contamination subtracted. It should be emphasized that the data are restricted to events with $\Delta < \Delta_{min} + 2\mu$ and $|\cos\theta_{\pi\pi}| < {\sim}0.4$. The smooth curve is the expected distribution for invariant phase space, obtained by adding the phase space curves for the three geometries (including the geometrical biases) after normalizing them rela-

tive to one another for the measured incident pion flux. The over-all normalization is arbitrary. The dip around 600 MeV results from insufficient overlap of the 17° and 27° efficiency curves.

In an attempt to remove the geometrical biases from the data, the experimental spectrum was divided by the distribution we would see if the production cross section were of the form

$$\frac{d^3\sigma}{d\Delta^2 d\cos\theta_{\pi\pi} dm^*} \propto \frac{\Delta^2}{(\Delta^2 + \mu^2)^2}; \qquad (1)$$

this choice of dependence on Δ and $\cos\theta_{\pi\pi}$ will be justified below. The resulting curve (Fig. 7) shows the dependence of the production cross section on m^* within our limited region of Δ and $\cos\theta_{\pi\pi}$.

The contribution of the ρ meson is evident from the broad peak in the data around 750 MeV, with a width on the order of 130 MeV. There is no evidence of the splitting of the ρ peak which has been reported by other groups. Away from the ρ, the data vary smoothly with respect to phase space and show no indication of any other resonances.
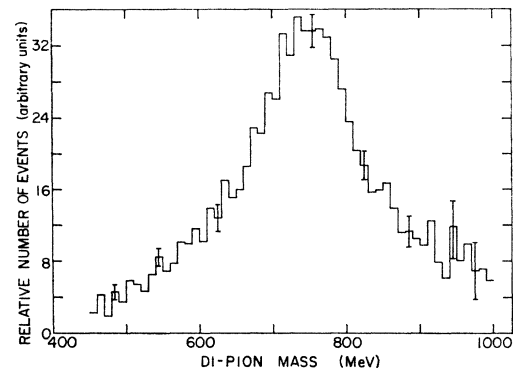

FIG. 7. Weighted dipion mass spectrum.

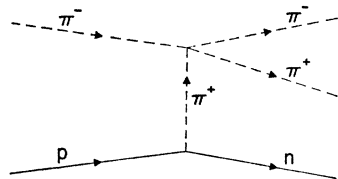FIG. 8. Diagram for one-pion exchange (OPE).

The positive G-parity assignment of the ω meson forbids it to decay to two pions except by electromagnetic interactions, but it has been pointed out that the relatively small ρ-ω mass difference could permit enhancement of the decay $\omega \to \pi^+\pi^-$ through mixing of the ρ and ω amplitudes.[8,9,13] A detailed analysis of these effects, however, depends strongly on the ρ and ω production mechanisms, which are not yet well understood. The situation is further complicated by the possibility of final state ρ-N and ω-N interactions,[17] which would influence the polarization vectors and the relative phases.

An examination of our data (Fig. 6) in the vicinity of the ω mass ($m_\omega = 784 \pm 0.9$ MeV; $\Gamma_\omega = 9.5 \pm 2.1$ MeV[18]) reveals no significant structure in this region. A smooth curve fit through the neighboring points (as shown in the inset in Fig. 6) indicates an excess of -3 ± 24 events in the region $775 < m^* < 795$ MeV. To set a limit on the branching ratio $R[\omega \to \pi^+\pi^-/\omega \to \pi^+\pi^-\pi^0]$, we have calculated that our data would contain 2200 ω's from the process $\pi^- + p \to \omega + n$, if we assume that all the ω's decay isotropically through the 2π mode. This figure is based on the production cross section of 1.4 mb and the production angular distribution observed in the charge-symmetric reaction $\pi^+ + n + (p) \to \omega^0 + p + (p)$.[19] Under the assumption that no interference occurs, our data then yield $R = (-0.1 \pm 1.1)\%$, or $R < 1.0\%$.

This limit is, of course, dependent upon the ω-decay angular distribution because of the restricted angular aperture of the apparatus. An assumed $\sin^2\theta_{\pi\pi}$ dependence (ω produced by ρ exchange) would increase the number of ω's we would detect by a factor of 2 to give $R < 0.5\%$.

The strong association of the ρ meson with low four-momentum transfer events has been observed in many experiments[1] and has led to a description of the interaction in terms of a peripheral process. The relatively large impact parameters in the initial system minimize the direct π-N interaction and lead to the observed backward peaking in the recoil nucleon angular distribution. The simplest mechanism for such a process is

the one-pion exchange (OPE) model; the diagram for this process is shown in Fig. 8.

Chew and Low[20] have pointed out a means of extracting the π-π cross section from the data if OPE is a contributing process. For the production cross section, they obtained the expression

$$\frac{\partial^3 \sigma}{\partial \Delta^2 \partial m^{*2} \partial \cos\theta_{\pi\pi}} \xrightarrow[\Delta^2 \to -\mu^2]{} F(\Delta^2, m^{*2}) \frac{\partial \sigma_{\pi\pi}}{\partial \cos\theta_{\pi\pi}}, \quad (2)$$

where

$$F(\Delta^2, m^{*2}) = \frac{f^2}{2\pi\mu^2} \frac{\Delta^2}{(\Delta^2 + \mu^2)^2} \frac{m^*(m^{*2}/4 - \mu^2)^{1/2}}{p_i^2}, \quad (3)$$

f is the pion-nucleon coupling constant, p_i is the incident pion momentum in the lab frame, and $\partial \sigma_{\pi\pi}/\partial \cos\theta_{\pi\pi}$ is the π-π cross section as a function of m^*, the c.m. total energy for π-π scattering. Since expression (2) is valid only at the pole $\Delta^2 = -\mu^2$ in the unphysical region, the proposed method is to divide the experimentally obtained cross sections by $F(\Delta^2, m^{*2})$ in the physical region; the resulting function is then extrapolated in Δ^2 to the pole to obtain the cross section for a real π-π scattering.

Unfortunately, such a procedure cannot be applied to our data because of our geometrical limitations. The extremely narrow region of Δ^2 to which we are confined for any particular value of m^* does not give us a sufficient lever arm for a reliable extrapolation. As an alternative, we have assumed (2) to be valid in the physical region for small Δ^2. Several authors[17,21] have proposed corrections to the Chew-Low expression for use in the physical region, but the changes in the dependence on Δ^2 are small enough that our geometrical biases prevent us from distinguishing between them with our data. Since we wish to compare our results with those of other experiments which obtain the total cross section from the unmodified Chew-Low expression, this procedure should not cause serious trouble.

As a first step in the investigation of the differential cross section, we have examined the π-π angular distributions in the limited region of $\cos\theta_{\pi\pi}$ available to us. The rapid fall of the efficiency function away from $\theta_{\pi\pi} = \frac{1}{2}\pi$ makes it difficult to say anything quantitative about the behavior of the distributions. For all values of m^* the data are consistent with a uniform distribution in $\cos\theta_{\pi\pi}$ over the region -0.4 to $+0.4$, but this does not negate the possibility of some angular dependence. There is no significant indication of any asymmetry about 90 deg.

We have calculated the differential π-π cross section $d\sigma_{\pi\pi}/d\cos\theta_{\pi\pi}$, averaged over the interval, $-0.2 < \cos\theta_{\pi\pi} < 0.2$. The values obtained are shown in Fig. 9. The procedure followed was to multiply Eq. (2) by the efficiency function $E(\Delta^2, m^*, \cos\theta_{\pi\pi})$ and integrate over

[17] M. H. Ross and G. L. Shaw, Phys. Rev. Letters 12, 627 (1964).
[18] N. Gelfand, D. Miller, M. Nussbaum, J. Ratau, J. Schultz, J. Steinberger, T. H. Tan, L. Kirsch, and R. Plano, Phys. Rev. Letters 11, 436, 438 (1963).
[19] T. C. Bacon, D. G. Hill, H. W. K. Hopkins, D. K. Robinson, and E. O. Salant, in Proceedings of the 12th Annual International Conference on High-Energy Physics Dubna, 1964 (Atomizdat, Moscow, 1965).

[20] G. F. Chew and F. E. Low, Phys. Rev. 113, 1640 (1959).
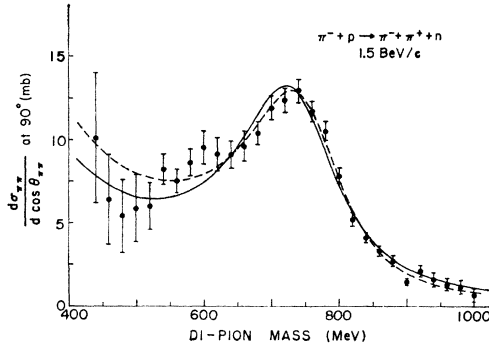[21] F. Selleri, Phys. Letters 3, 76 (1962).

FIG. 9. $\partial\sigma_{\pi\pi}/\partial\cos\theta_{\pi\pi}$, averaged over the interval $-0.2<\cos\theta_{\pi\pi}$ <0.2. The curves show fits obtained with a Breit-Wigner resonance plus a background term varying as λ^2. Solid curve: no resonant-nonresonant interference term, $m_0=736$ MeV, $\Gamma=176$ MeV, 1.5% χ^2 probability. Dashed curve: with interference term, $m_0=753$ MeV, $\Gamma=170$ MeV, 47% χ^2 probability. Both fits show an 11 mb resonant contribution to the cross section.

the intervals $\Delta_{min}<\Delta_{min}+2\,\mu$ and $-0.2<\cos\theta_{\pi\pi}<0.2$, assuming $d\sigma_{\pi\pi}/d\cos\theta_{\pi\pi}$ to be independent of $\cos\theta_{\pi\pi}$ in this region. Dividing the data from these regions of Δ and $\cos\theta_{\pi\pi}$ by the resulting function yields the desired cross section.

The values were calculated separately for the data at each geometry and averaged in the overlapping regions to obtain the points shown. The points obtained at each geometry were in good statistical agreement in the regions of m^* where they overlapped one another. Since $F(\Delta^2,m^{*2})$ as defined in (3) explicitly contains $1/p_i^2$, an average value of $1/p_i^2$ as a function of m^* was determined from the data for use in this calculation. These values agreed well with the expected values from the Monte Carlo calculations, and we feel that this procedure did not contribute any significant error to the cross section. The points below 530 MeV are somewhat questionable since the corrections for multiple-pion production events amounted to 30–50% in this region (see Fig. 5).

A partial-wave expansion of the π-π cross section indicates that a real $T=1$, $J=1$ π-π resonance at 750 MeV should contribute a maximum of only 2.4 mb to the differential cross section we have calculated if we neglect interference terms with other partial waves.[22] However, a previous measurement[5] of the total π-π scattering cross section at our energy (calculated in the physical region with the unmodified Chew-Low expression) has shown a maximum contribution from the ρ of 56 ± 8 mb, instead of the 120 mb expected from the partial-wave expansion. Scaling the figure of 2.4 mb accordingly, we would expect to find the ρ contributing

only 1.1 ± 0.1 mb to our data, instead of the rather large bump evident in Fig. 9.

To estimate the resonant contribution to the cross section, we have attempted to fit the data with an expression of the form

$$\frac{d\sigma(m^*)}{d\cos\theta_{\pi\pi}}\bigg|_{90°} = \lambda^2\left|a_1+a_2\frac{\frac{1}{2}\Gamma}{m^*-m^*_0+i\Gamma/2}\right|^2; \quad (4)$$

fits were made both with and without interference terms. The resulting curves, shown in Fig. 9, are not particularly good fits; the background under the resonance appears to fall off more rapidly than λ^2. However, both fits indicate a resonant contribution of 11 ± 1 mb to the cross section which, even in view of the poor fits obtained, is difficult to reconcile with the expected value of 1.1 mb from above.

It has been pointed out by Ross and Shaw[17] that final state ρ-N interactions could produce a spin-orbit coupling which would lead to a depolarization of the ρ. This process would introduce an isotropic component into the ρ decay and greatly increase the number we would see around 90 deg. If we assume that this effect is responsible for an enhancement of the ρ in our data, the ρ decay intensity can be expressed in the form $a+b$ $\cos^2\theta_{\pi\pi}$. Under the assumption that only the $J=1$ state is resonant, our data then require $a/b\approx0.06$ to account for the 11-mb contribution found above, while the simple OPE model gives $a/b=0$.

We cannot on the basis of our data exclude the possibility that another resonant state is present in addition to the ρ. A $T=0$ s-wave resonance at 750 MeV would contribute 4–8 mb to the cross section, depending on the corrections to the OPE model. Since these corrections should be quite significant at our energy,[17] we tend toward the lower figure of 4 mb, which would still not account for the peak we see without some depolarization of the $J=1$ resonance. The ratio $a/b\approx0.06$ is accordingly somewhat arbitrary, since we can say very little about the possibility of other resonant states involved in the interaction.

Several groups have performed phase-shift analyses of the π-π cross section in the ρ region,[23,24] although their data were obtained at higher energies than ours. In addition to the ρ resonance, their results indicate the presence of a large and possibly resonant $T=0$ s-wave contribution. However, differential cross sections calculated from several of these phase shift sets were in poor agreement with our data, and, in particular, did not show the strong peak we observed. This discrepancy can probably be accounted for by the increased effect of the final state interactions at our lower energy; the presence of these non-OPE processes also casts some

---

[22] Symmetry considerations restrict states with $T=1$ to odd J, and states with $T=0$ or 2 to even J; the symmetry of the spherical harmonics causes interference terms to vanish between $T=1$ states and $T=0$ or 2 states since we are looking at 90°. In the cross section we have calculated, a $T=1$, $J=1$ resonance can only interfere with other $T=1$ states with J greater than or equal to 3.

[23] V. Hagopian, Ph.D. thesis, University of Pennsylvania, 1963 (unpublished); V. Hagopian and W. Selove, Phys. Rev. Letters 10, 533 (1963).
[24] Y. Y. Lee, University of Michigan, Technical Report 04938-1-T, 1964 (unpublished).

doubt on the validity of a phase shift analysis unless they are properly taken into account.

The characteristic feature of the OPE model is a strong peaking in the four-momentum transfer spectrum at $\Delta^2 = \mu^2$, which is near the lower boundary of the kinematically allowed region. The proposed modifications to the OPE model for use in the physical region change the dependence on Δ^2 slightly from that given in expression (2), but the spectrum retains the same general shape. Since our apparatus was designed to select primarily low momentum transfer events, our geometrical biases vary rapidly with Δ^2 and make it impossible for us to distinguish between these various distributions with our data.

Figure 10 shows the momentum transfer distributions obtained for several regions of m^*. The solid curves show the spectra predicted by the unmodified OPE model; the phase space distributions are shown for comparison as dashed curves. The strong effect of the geometrical biases is illustrated by the phase space curves, which would rise linearly with Δ for $\Delta > \Delta_{min}$ if there were no biases. A generally good agreement with OPE is evident, but there is some indication that the data are more sharply peaked toward low momentum transfer than is predicted by OPE.

Treiman and Yang have pointed out another condition which the data must satisfy if OPE is the dominant mechanism.[25] Since the exchanged π is spinless, no angular information can be transmitted between the two vertices of the diagram. The physical consequences of this situation can best be visualized in the dipion rest system (see Fig. 11). In this reference system, the momentum vectors of the incident proton and the recoil neutron determine a plane; a second plane is defined by the vectors of the incident and two decay pions. The planes intersect along the line determined by the incident and virtual pion momentum vectors. OPE then
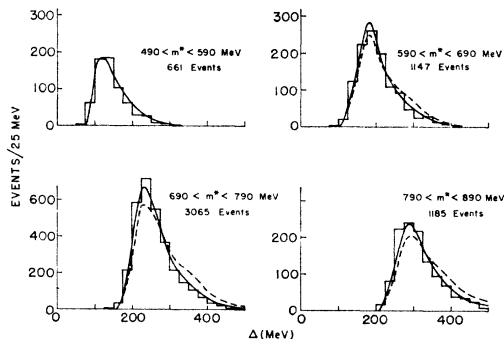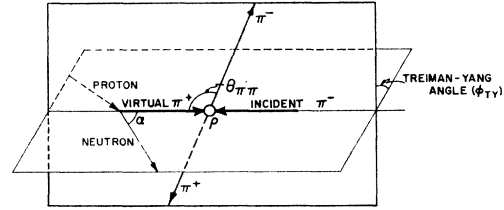

FIG. 11. Illustration of the Treiman-Yang angle in the dipion rest frame.

implies that Φ_{TY}, the Treiman-Yang angle, must be uniformly distributed.

We have plotted the distributions in Φ_{TY} in Fig. 12 for several regions of m^* (defining the angle over the interval $-\pi < \Phi_{TY} < \pi$, we consider $|\Phi_{TY}|$). Again the detection efficiency has a strong effect on the spectra; the smooth curves represent the distributions we would see if the data followed the OPE model, with an isotropic distribution in Φ_{TY}. The data follow the general shape of the expected distributions, but in every case there is a depletion of events for Φ_{TY} near 0 and π, indicating some violation of OPE. However, because of our geometrical restriction on $\cos\theta_{\pi\pi}$, there is a correlation between Φ_{TY} and the π-N effective masses, such that isobar formation could strongly affect the Treiman-Yang angular distributions we observe.

The $\pi^{\pm}$–n effective mass $(M_{\pm})$ can be expressed as

$$M_{\pm}^2 = \tfrac{1}{2}(W^2 + M^2 - m^{*2} + 2\mu^2) \pm 2\mathbf{p}_n \cdot \mathbf{p}_\pi, \qquad (5)$$

where $\mathbf{p}_n$ and $\mathbf{p}_\pi$ are the momenta of the neutron and outgoing negative pion respectively in the π-π rest system (see Fig. 11), and W is the total energy in the production c.m. system. For fixed values of m^{*2} and Δ^2, the magnitudes p_n and p_π are constant. Since our data are restricted to small values of $\cos\theta_{\pi\pi}$, the scalar product in (5) to a good approximation is then proportional to $\cos\Phi_{TY}$, which is the only variable remaining. Under
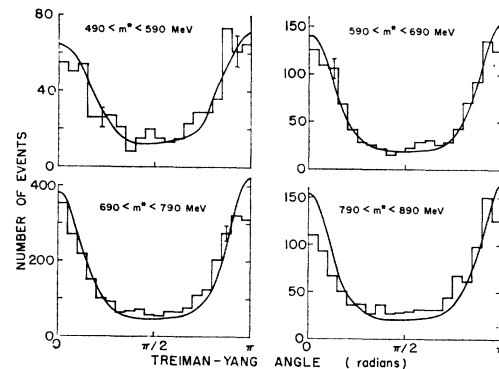

FIG. 10. Momentum transfer distributions for several regions of m^*. The solid curves show the OPE prediction; the dashed curves are phase space. For $490 < m^* < 590$ MeV, the phase-space curve is not significantly different from OPE and is not shown. Each curve is normalized to the same number of events as the associated histogram.

FIG. 12. Treiman-Yang angular distributions for several regions of m^*. The smooth curves show the spectra we would see due to the geometrical biases if the interaction were independent of Φ_{TY}, following OPE.
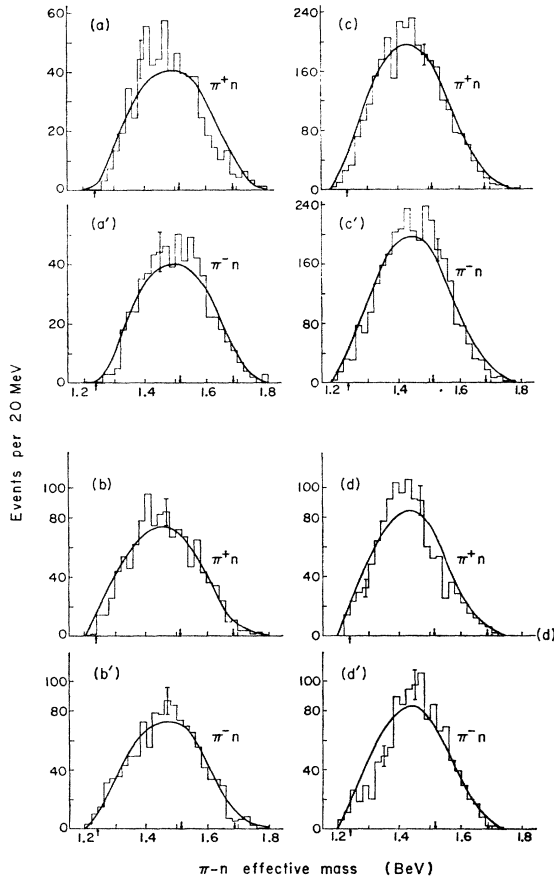
[25] S. B. Treiman and C. N. Yang, Phys. Rev. Letters **8**, 140 (1962).

FIG. 13. π^+-n and π^--n effective mass distributions.

(a,a')490$<m^*<$590 MeV; (b,b')590$<m^*<$690 MeV; (c,c')690$<m^*<$790 MeV; (d,d')790$<m^*<$890 MeV.

The predicted OPE distributions are shown as smooth curves, each normalized to the same number of events as the associated histogram.

these conditions, (5) then reduces to the form

$$M_{\pm}^2 = a \pm b \cos\Phi_{TY},\qquad (6)$$

where a and b are essentially constant for any limited range in m^{*2} and Δ^2. We note that there is also a correlation between M_+^2 and M_-^2 in our data.

The π^+-n and π^--n effective mass distributions for several regions of m^* are shown in Fig. 13. Again our geometrical cutoffs limit the data to a fraction of the kinematically allowed region, with our maximum sensitivity for π-N masses of 1.4–1.5 BeV. The smooth curves show the distributions expected from the OPE model, normalized to the same number of events. There is no indication in either the π^+-n or π^--n spectra of any contribution from the N^* (1238), which is just within our detectable range, or of the N^* (1512) and N^* (1688). In all cases, the data are more sharply peaked than are the OPE curves, which, in view of the correlations pointed out above, is consistent with the observed excess of events with Φ_{TY} in the neighborhood of $\frac{1}{2}\pi$. There also appears to be a shift in the position of the peak between the π^+-n and π^--n distributions, particularly for 490$<m^*<$590 MeV and 790$<m^*<$890 MeV.

Evidence has recently been reported of a $T=\frac{1}{2}$ π^--p state with an effective mass of about 1.4 BeV.[26] While our data are not sufficient to permit identification of such a state, its presence would account for our observed departures from OPE in the $M_{\pm}$ and Φ_{TY} distributions. Because of the M_+-M_- correlation mentioned above, the formation of a π^+-n state at 1.4 BeV would introduce a corresponding peak in the π^--n spectrum at a slightly higher mass, producing a slight shift in the peak as is observed outside the ρ region. The excess events near the center of the π-N distributions would also yield the observed Φ_{TY} spectra.

ACKNOWLEDGMENTS

[26] P. Bareyre, C. Bricman, G. Valladas, G. Villet, J. Bizard, and J. Seguinot, Phys. Letters 8, 137 (1964).
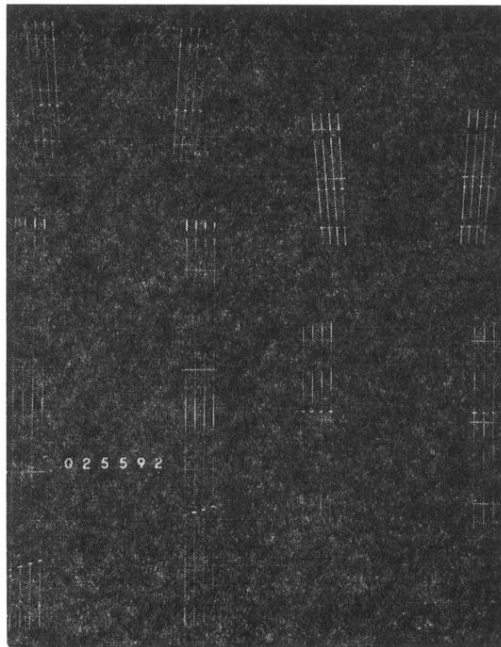
FIG. 3. Typical data picture, showing a negative pion passing through one spectrometer.